

Effect of Particle Erosion on the External Collapse Pressure of a Steel Production Casing Used in Oil and Gas Wells

Nick Boer

18-12-2017

Internship Report
Faculty of Mechanical Engineering and Aerospace Engineering
Institut Teknologi Bandung

Supervisor Institut Teknologi Bandung: Dr.Ir. Bagus Budiwantoro
Supervisor University of Twente: Dr.Ir. Rob Bosman

Preface

In this report the result of a study concerning the effect of particle erosion on the structural integrity of steel production casings used in oil and gas wells is presented. The effect of erosion profiles on the external collapse pressure of a production casing is evaluated using FEA (Finite Element Analysis) simulations. The research is carried out as an internship assignment as a part of the Mechanical Engineering Master's programme of University of Twente (UT, The Netherlands), in a time span of eleven weeks.

The internship is carried out at Institut Teknologi Bandung (ITB, Indonesia) under supervision of Dr.Ir. Bagus Budiwantoro and is initiated as a cooperation between the UT and ITB. The idea of the research subject was brought up by my UT-supervisor Dr.Ir. Rob Bosman and his colleague Dr.Ir. Rihard Pasaribu (both employees of Royal Dutch Shell). I would like to thank Dr.Ir. Bagus Budiwantoro for his hospitality, advice and the opportunity to carry out this internship at the Mechanical Engineering and Aerospace Engineering Faculty of ITB. Besides, I would like to thank Dr.Ir. Rob Bosman and Dr.Ir. Rihard Pasaribu for offering the opportunity and their assistance before and during the internship period.

Bandung, 21-12-2017

Nick Jan Boer

Summary and Conclusions

In the oil industry it is of great importance to accurately predict the external collapse pressure of the Oil Country Tubular Goods (OCTG) used in well applications as the collapse of a casing tube used in an oil well can lead to important economic losses and serious ecological damages. In this study the effect of solid particle erosion on the external collapse pressure of a production casing is evaluated by the use of FEA collapse simulations.

In the literature study, two analytical models are proposed to calculate the external collapse pressure: the *Shell Collapse Pressure Formula* and the *American Petroleum Institute Collapse Equations*. The API equations provide accurate results and are used in well design, so these formulas are used for model validation in this research.

The particle material, angle of impingement, particle impact velocity and particle size determine which erosion mechanism is active. In addition to these factors, there are other factors that influence the erosion rate, of which a list is provided and the effect of each factor on the erosion rate is discussed. No general erosion prediction model is present in literature that is suitable for practical use. This is because some aspects of the erosion mechanism are not fully understood yet and further research is required to develop a consistent set of physical parameters that can describe the erosion situation.

A uniform cross-section model with a nominal outside diameter of 177.8 mm, a wall thickness of 9.36 mm and an ovality of 0.18% is used to represent the production casing. The perforation design is as follows: 26 SPM, 90 degree phasing, 13 mm tunnel diameter. The used material is Grade L80 steel.

Simulations are done with common steel casing geometries (without the perforation tunnels) to examine the validity of the FEA model. The FEA collapse pressure is compared to the API collapse pressure. Three steel casing geometries are used for model validation, which results in FEA collapse pressure over API collapse pressure ratios of 1.23, 1.52 and 1.33.

The effect of six erosion profiles on the external collapse pressure is evaluated using FEA simulations: three profiles with a maximum erosion depth of 10% and three profiles with a maximum depth of 25%. For both erosion intensities, the separate effect of erosion profile characteristics is evaluated using the following profiles: a profile with both wall thickness decrease and perforation tunnel diameter increase, a profile with wall thickness decrease only and a profile with perforation tunnel diameter increase only.

The effect of the erosion profiles on the external collapse pressure is evaluated by comparing the FEA collapse pressure with the FEA collapse pressure of the uneroded casing. As expected, the erosion profiles with both the wall thickness decrease and the tunnel diameter increase show the largest drop in collapse pressure (decrease of 5% for the 10% profile and 11% for the 25% profile). Furthermore, it can be concluded that the effect of decreased wall thickness on the external collapse pressure is bigger than the effect of the increased tunnel diameter.

List of Symbols

d_{max}	=	Maximum outer diameter [mm]
d_{min}	=	Minimum outer diameter [mm]
d_o	=	Nominal outer diameter [mm]
E	=	Young's modulus [GPa]
ϵ_{eng}	=	Engineering strain [-]
ϵ_{true}	=	True plastic strain [-]
F_n	=	Material constant used in API collapse formulas [-]
L	=	Length [mm]
ν	=	Poisson ratio [-]
Ov	=	Ovality percentage (%)
P_{co}	=	Collapse pressure [MPa]
$P_{co,API}$	=	API collapse pressure [MPa]
$P_{co,el}$	=	Collapse pressure elastic collapse [MPa]
$P_{co,FEA}$	=	FEA collapse pressure [MPa]
$P_{co,pl}$	=	Collapse pressure plastic collapse [MPa]
P_e	=	External pressure [MPa]
P_i	=	Internal pressure [MPa]
r_i	=	Nominal inner radius [mm]
r_o	=	Nominal outer radius [mm]
σ_{eng}	=	Engineering stress [MPa]
σ_r	=	Radial stress [MPa]
σ_t	=	Tangential stress [MPa]
σ_{true}	=	True stress [MPa]
σ_y	=	Yield strength [MPa]
$(\sigma_y)_e$	=	Effective yield strength [MPa]
t	=	Nominal wall thickness [mm]
u_{max}	=	Maximum total displacement [mm]
V_L	=	Particle impact velocity [m/s]

Contents

Preface	i
Summary and Conclusions	ii
List of Symbols	iii
1 Introduction	2
2 Literature study	4
2.1 Analytical Collapse Pressure Calculation	4
2.1.1 Shell Collapse Pressure Formula	4
2.1.2 American Petroleum Institute Collapse Formulas	5
2.2 Erosion Mechanisms	9
2.3 Factors Influencing Erosion Rate	12
2.4 Erosion Rate Prediction Models	15
3 Production Casing and Erosion Profiles	16
3.1 Production Casing Geometry	16
3.2 Production Casing Material Properties	19
3.3 Erosion Profiles	20
4 Collapse Simulations	24
4.1 FEA Model Description	24
4.2 Model Validation	28
4.3 Production Casing Collapse Simulations	31
5 Conclusions	33
6 Discussion and Recommendation	34
A Hosting organization and role	37
Bibliography	38

Chapter 1

Introduction

In the oil industry it is of great importance to accurately predict the external collapse pressure of the Oil Country Tubular Goods (OCTG) used in well applications. Piping collapse is considered as the *local buckling mode*, an example of this buckling mode is depicted in Figure 1.1. The collapse of a casing tube used in an oil well can lead to important economic losses and serious ecological damages. External pressure collapse tests are performed by manufacturers of so called high collapse casings to guarantee a minimum service performance. Sand production during well exploitation causes erosion and thus changes the geometrical properties of the casing, which affects the structural integrity. The lowest part of the well – the production casing – is particularly important considering the aforementioned phenomenon. External pressure is at the highest level at the bottom of the well and the production casing is subject to high pressure high velocity flow, causing severe erosion. Collapse of the production casing may lead to a reduced production rate of the well or even to a non-producing well. Objective of this research is to predict the effect of particle erosion on the external collapse pressure of the production casing using FEA simulations.



Figure 1.1: Local buckling of a steel casing used in oil/gas well applications (Dvorkin and Toscano, 2003)

Firstly, in Chapter 2 a literature study is presented on the local pipe buckling and erosion phenomena. Analytical models are presented that are suggested by literature to predict the collapse pressure of steel pipes, as well as the factors that influence the collapse pressure. The erosion phenomenon is discussed in general, as well as the parameters that determine the erosion rate. Besides, the current state of literature on erosion prediction models is discussed.

Secondly, the geometry and material properties of a typical production casing is presented in Chapter 3. Based on the knowledge on erosion that is gathered in Chapter 2, an erosion profile is assumed that is used in the FEA simulations.

Chapter 4 starts with a description of the FEA model configurations used in the collapse simulations. As there is no experimental data available of the collapse of production casings, the model is validated first by simulating the collapse of a uniform cross-section pipe. The collapse pressure predicted by the simulation is compared with the collapse pressure that is calculated using the analytical models discussed in Chapter 2. After validation of the model, the last step is to predict the collapse pressures of the uneroded and the eroded production casings.

A conclusion on this research can be found in Chapter 5, followed by a discussion and recommendations for further research in Chapter 6.

Chapter 2

Literature study

The results of a literature study are presented in this chapter. The first paragraph is about the phenomenon of global pipe buckling, also called 'pipe collapse'. In Paragraph 2.2, the different ways in which erosion can occur (erosion mechanisms) are presented. Finally, the influence of several factors on the erosion rate is discussed in Paragraph 2.3.

2.1 Analytical Collapse Pressure Calculation

In this paragraph two possibilities to analytically calculate the collapse pressure of a tube are presented. In the first paragraph the *Shell* collapse pressure formula is discussed, which gives a rough estimate of the collapse pressure. Secondly, the equations provided by the American Petroleum Institute (API) are presented. These equations give a more accurate prediction of the collapse pressure and are widely used as guidelines for well design.

2.1.1 Shell Collapse Pressure Formula

Kyriakides and Corona (2007) provide a formula to calculate a quick first estimate of the collapse pressure. This formula is called the *Shell* collapse pressure formula and is given by:

$$P_{co} = \left(\frac{1}{P_{co,el}^2} + \frac{1}{P_{co,pl}^2} \right)^{-1} \quad (2.1)$$

Buckling can occur in different 'buckling regions', depending on the geometrical properties of a tube. Two buckling regions are elastic buckling and plastic buckling. Equations for elastic buckling collapse pressure $P_{co,el}$ and the plastic buckling collapse pressure $P_{co,pl}$ are given by:

$$P_{co,el} = \frac{2E}{(1-\nu^2)} \left(\frac{t}{d_o} \right)^3 \quad (2.2)$$

and

$$P_{co,pl} = \frac{2\sigma_y t}{d_o} \quad (2.3)$$

The *Shell* collapse pressure equation is obtained by combining above two expressions. The equation can be used when the collapse region is unknown and it is based on the idea that elastic buckling occurs at $P_{co,el}$ and plastic buckling at $P_{co,pl}$. In this way a rough estimate of the collapse pressure P_{co} can be calculated. Besides the fact that only a rough estimation is obtained, other limitations of this formula are that it does not take into account influencing factors like residual stresses, geometrical imperfections (ovality, eccentricity) and material imperfections.

2.1.2 American Petroleum Institute Collapse Formulas

The API (American Petroleum Institute) provides equations to predict the main performance properties of a steel casing: burst pressure, collapse pressure and axial tension (Bull, 1985). These equations are recommended for use in well design. In this subsection, the API analytical formulas to predict the collapse pressure of a casing are given.

It turns out that a simplified Free Body Diagram is not sufficient to determine the external collapse pressure of a pipe. However, as can be seen in Bourgoyne et al. (1991), it is possible to establish an analytical expression using the classical elasticity theory. Figure 2.1 shows a 2D wall stress situation with external pressure P_e and internal pressure P_i . Using the classical elasticity theory, the radial and tangential stresses σ_r and σ_t at radius r can be determined with:

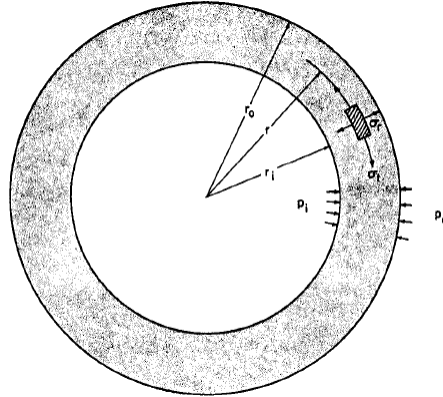


Figure 2.1: Cross-section with external pressure and internal pressure (Bourgoyne et al., 1991)

$$\sigma_r = \frac{P_i r_i^2 (r_o^2 - r^2) + P_e r_o^2 (r^2 - r_i^2)}{r^2 (r_o^2 - r_i^2)} \quad (2.4)$$

and

$$\sigma_t = \frac{P_i r_i^2 (r_o^2 + r^2) - P_e r_o^2 (r_i^2 + r^2)}{r^2 (r_o^2 - r_i^2)} \quad (2.5)$$

The stress is at maximum in the tangential direction for both the burst and collapse situation of the pipe. Besides this, the stress is highest at the inside of the hoop. When assuming zero internal pressure and $r = r_i$, the equation for the tangential stress reduces to:

$$\sigma_t = \frac{2P_e r_o^2}{t(r_o + r_i)} \quad (2.6)$$

When using the effective compressive yield strength for σ_t , rearranging terms of the above equation leads to the following formula for the collapse pressure P_{co} :

$$P_{co} = 2(\sigma_y)_e \left[\frac{d_o/t - 1}{(d_o/t)^2} \right] \quad (2.7)$$

The collapse pressure equation that is given above can be used to calculate the collapse pressure in the so called *yield strength collapse* region. It has been shown experimentally that, for oil-well casing, this type of collapse only occurs at the lower range of d_o/t values. The d_o/t ratio indicates the relative wall thickness of the pipe. A high value for this ratio indicates a small relative wall thickness.

Besides yield strength collapse, the other collapse regions are: plastic collapse, transition collapse and elastic collapse. The d_o/t ratio determines the type of collapse, as can be seen in Figure 2.2. Because material parameters are included in the formula to calculate the d_o/t ratio, the boundaries for the different collapse type ranges differ for each steel grade.

The upper limit of the yield-strength collapse range is calculated using:

$$d_o/t = \frac{\sqrt{(F_1 - 2)^2 + 8(F_2 + F_3/(\sigma_y)_e)} + (F_1 - 2)}{2(F_2 + F_3/(\sigma_y)_e)} \quad (2.8)$$

The F -variables are tabulated constants that differ for each API recognized steel grade. In Figure 2.3, the F -values for several steel grades are given. The effective yield strength $(\sigma_y)_e$ used in the formula is equal to the minimum yield strength when no axial stresses are present.

At high d_o/t ratios, the pipe structure can collapse under lower pressures due to geometric instability. The collapse ratio for pipes in the elastic collapse region is calculated with:

Grade*	←Yield Strength→ Collapse	←Plastic→ Collapse	←Transition→ Collapse	←Elastic→ Collapse
H-40	16.40	27.01	42.64	
-50	15.24	25.63	38.83	
J-K-55 & D	14.81	25.01	37.21	
-60	14.44	24.42	35.73	
-70	13.85	23.38	33.17	
C-75 & E	13.60	22.91	32.05	
L-80 & N-80	13.38	22.47	31.02	
C-90	13.01	21.69	29.18	
C-95	12.85	21.33	28.36	
-100	12.70	21.00	27.60	
P-105	12.57	20.70	26.89	
P-110	12.44	20.41	26.22	
-120	12.21	19.88	25.01	
-125	12.11	19.63	24.46	
-130	12.02	19.40	23.94	
-135	11.92	19.18	23.44	
-140	11.84	18.97	22.98	
-150	11.67	18.57	22.11	
-155	11.59	18.37	21.70	
-160	11.52	18.19	21.32	
-170	11.37	17.82	20.60	
-180	11.23	17.47	19.93	

Figure 2.2: Range for d_o/t for various collapse type regions when axial stress is zero) (Bourgoyne et al., 1991)

$$P_{co} = \frac{46.95 \times 10^6}{(d_o/t)(d_o/t - 1)^2} \quad (2.9)$$

The lower limit of the elastic collapse region is calculated with:

$$d_o/t = \frac{2 + F_2/F_1}{3F_2/F_1} \quad (2.10)$$

The collapse rating for plastic collapse, which is just above the yield strength region, is predicted with:

$$P_{co} = (\sigma_y)_e \left(\frac{F_1}{d_o/t} - F_2 \right) - F_3 \quad (2.11)$$

The upper limit of the plastic collapse region is determined with:

$$d_o/t = \frac{(\sigma_y)_e(F_1 - F_4)}{F_3 + (\sigma_y)_e(F_2 - F_5)} \quad (2.12)$$

Grade*	Empirical Coefficients				
	F_1	F_2	F_3	F_4	F_5
H-40	2.950	0.0465	754	2.063	0.0325
-50	2.976	0.0515	1,056	2.003	0.0347
J-K 55 & D	2.991	0.0541	1,206	1.989	0.0360
-60	3.005	0.0566	1,356	1.983	0.0373
-70	3.037	0.0617	1,656	1.984	0.0403
C-75 & E	3.054	0.0642	1,806	1.990	0.0418
L-80 & N-80	3.071	0.0667	1,955	1.998	0.0434
C-90	3.106	0.0718	2,254	2.017	0.0466
C-95	3.124	0.0743	2,404	2.029	0.0482
-100	3.143	0.0768	2,553	2.040	0.0499
P-105	3.162	0.0794	2,702	2.053	0.0515
P-110	3.181	0.0819	2,852	2.066	0.0532
-120	3.219	0.0870	3,151	2.092	0.0565
-125	3.239	0.0895	3,301	2.106	0.0582
-130	3.258	0.0920	3,451	2.119	0.0599
-135	3.278	0.0946	3,601	2.133	0.0615
-140	3.297	0.0971	3,751	2.146	0.0632
-150	3.336	0.1021	4,053	2.174	0.0666
-155	3.356	0.1047	4,204	2.188	0.0683
-160	3.375	0.1072	4,356	2.202	0.0700
-170	3.412	0.1123	4,660	2.231	0.0734
-180	3.449	0.1173	4,966	2.261	0.0769

Figure 2.3: Empirical coefficients used for collapse pressure calculation (Bourgoyne et al., 1991)

Finally, the collapse rating of the transition collapse type is calculated by using:

$$P_{co} = (\sigma_y)_e \left(\frac{F_4}{d_o/t} - F_5 \right) \quad (2.13)$$

The equations given in this section are used to validate the FEA model to simulate the collapse of the uneroded and eroded production casings (see Paragraph 4.2).

2.2 Erosion Mechanisms

Erosive and abrasive wear are both types of wear that is caused by contact between a particle and a surface of a solid material. The loss of material due to abrasive wear can be attributed to the passage of hard particles against a surface, while erosive wear is defined as the loss of material due to the impact of particles against a solid surface. Erosion in the steel casings used for oil/gas exploitation is caused by impacting particles in the fluid flow, also called particle erosion. This type of erosion will be considered in the remainder of this research. In this section, the fundamental mechanism(s) involved in particle erosion will be discussed.

Erosive wear cannot be described by one single mechanism. In fact, there are several types of particle erosion processes known and the properties of the particle-eroding material mechanism determines the type of mechanism that is active. Parameters that influence the type of erosion mechanism are: particle material, angle of impingement, particle impact velocity and the particle size. The mechanisms of erosive wear, which are illustrated in Figure 2.4, are (Stachowiak and Batchelor, 2013):

- (a) Abrasion at low impact angles
- (b) Surface fatigue during low speed and high impingement angle impact
- (c) Brittle fracture or multiple plastic deformation at medium speed and large impact angle
- (d) Surface melting at high impact speeds
- (e) Macroscopic erosion with secondary effects
- (f) Crystal lattice deformation from impact by atoms

Abrasion at low impact angles

This ‘cutting’ or ‘micromachining’ mechanism was firstly introduced by Finnie (1960), and is considered as a pioneering effort in this research area. He suggested that an impacting particle under oblique impact cuts/deforms a part of the surface and then leaves the surface with less kinetic energy. This mechanism is only active in ductile materials and when the impact angle is relatively low. At higher attack angles, the horizontal component of the velocity is too small to create a sufficient shear force for the ‘cutting’ action.

Surface fatigue during low speed and high impingement angle impact

Other than the cutting mechanism, the ‘fatigue mechanism’ imposes that erosion is caused by the nucleation and growth of a crack under a cyclic impact condition. This mechanism becomes active when the speed of the particle is insufficient to deform the material plastically. Besides, this mechanism occurs at higher impact angles, especially with brittle materials.

Brittle fracture or multiple plastic deformation at medium speed and large impact angle

At large impingement angles, no shear action can be activated which cuts away a volume as proposed by the cutting mechanism. However, when the velocity of the part is high enough, plastic deformation or brittle fracture of the eroded surface will occur. When the material is ductile, plastic deformation of the surface will result in a crater under the forming of lips. These lips will fracture under subsequent impacts. Brittle materials show erosion by brittle fracture at each impact, which is a very persistent type of erosion.

Surface melting at high impact speeds

At very high speeds, the kinetic energy of the particles can be sufficiently high to cause melting of the eroded surface. This is an erosion mechanism that is rarely observed in industrial applications.

Macroscopic erosion with secondary effects

When the size of the eroding particle is extremely big (e.g. the bombardment of a meteorite), the macroscopic erosion mechanism becomes active. With this mechanism, several macroscopic effects are observed, such as superplastic flow, melting of the surface and the formation of a debris cone around the impact crater.

Crystal lattice deformation from impact by atoms

On the other side of the extremity, when the impacting particles are very small, erosion may occur which is caused by the deformation of the crystal lattice of the material. For instance, impacting atoms may cause erosive wear on Low Earth Orbit satellites (Stachowiak and Batchelor, 2013).

To conclude, a remark on the relation between the impingement angle of the particle and the type of active erosion mechanism is made. When erosion shows its maximum at low impingement angles, it can be concluded that the 'ductile erosive mechanism' of cutting is active. When the maximum wear rate is found at high impact angles, 'brittle erosion' is active. It is not always possible to predict the type of erosion mechanism that occurs based on the known material and flow parameters. Scanning Electron Microscopy (SEM) examination of eroding surfaces can be helpful to find out which erosion mechanism is active.

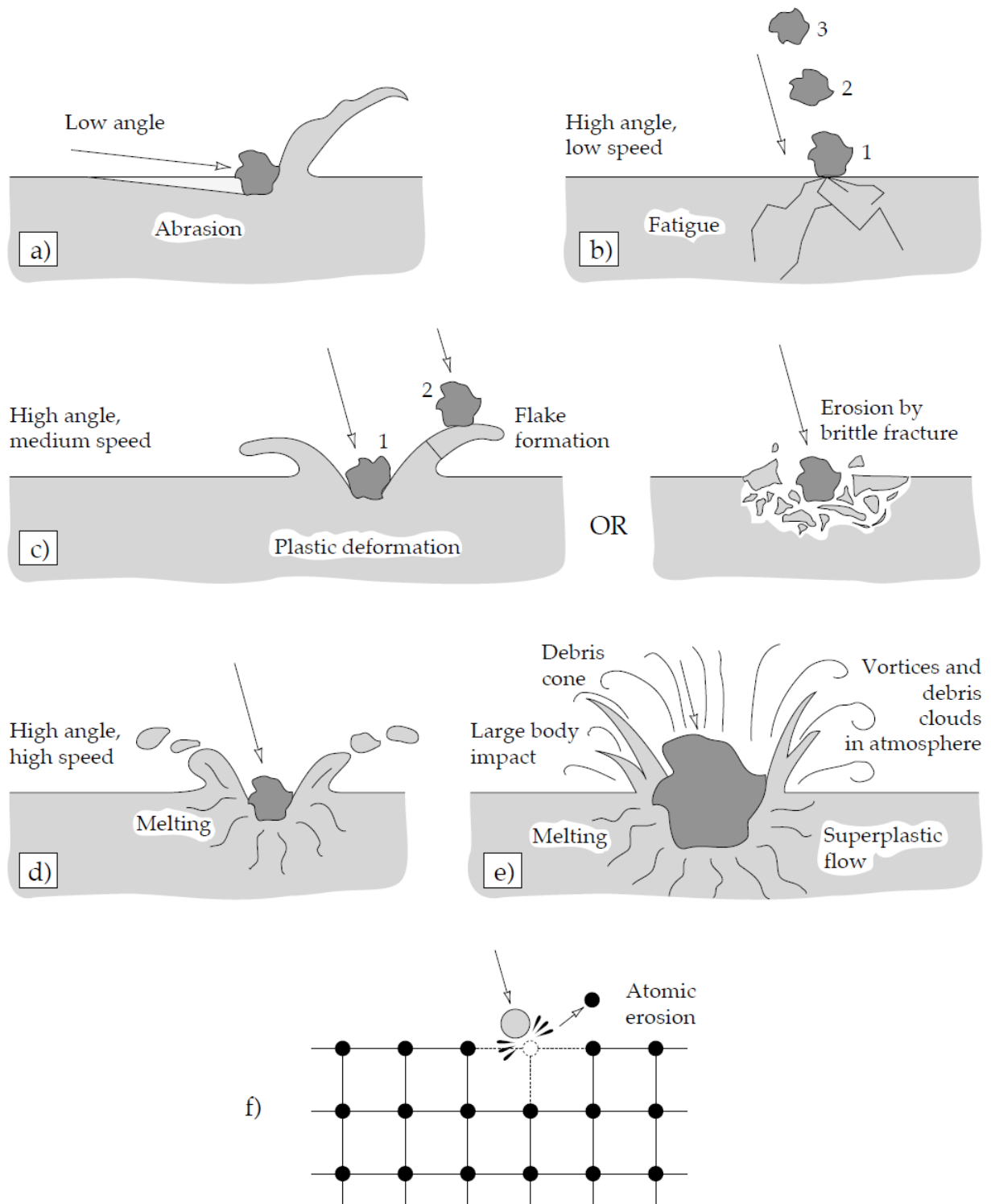


Figure 2.4: Mechanisms of erosion (Stachowiak and Batchelor, 2013)

2.3 Factors Influencing Erosion Rate

Erosion is a complex phenomenon that is affected by a lot of factors. Literature research is done in order to get a complete list of factors influencing erosion. This list is given in this paragraph and the effect of each parameter on the erosion rate is discussed separately.

The following factors, which are divided into four subclasses, are directly or indirectly influencing the erosion rate (Parsi et al., 2014; Stachowiak and Batchelor, 2013; Finnie, 1960; Pereira et al., 2014; Kleis and Kulu, 2007):

Particle properties

- Size
- Shape
- Density
- Hardness

Fluid properties

- Velocity
- Density
- Viscosity

Eroding material properties

- Hardness
- Ductility
- Toughness
- Strength

Other factors

- Piping geometry
- Particle concentration
- Temperature

Particle size

The size of the impacting particle has a lot of influence on the erosion rate. Large particles cause a larger erosion rate than small particles. The reason for this is that, when considering two particles with the same speed, the larger particle has a larger kinetic energy. In general, the relation between erosion rate and particle size can be described by (Parsi et al., 2014):

$$\text{Erosion Rate} \propto (\text{Particle Size})^n \quad (2.14)$$

Most researchers observed a linear relation ($n=1$) between the erosion rate and the particle size (Gandhi and Borse, 2002; Elkholy, 1983; Clark, 1991). However, Desale et al. (2009) suggest that the value for n ranges from 0.3 to 2.0, depending on experimental conditions, difference in material properties, particle velocity and other parameters.

Another observation on the relation between erosion ratio and particle size is depicted in Figure 2.5. In this figure, it can be seen that the erosion rate increases with increasing particle size, up to a certain level (the curve flattens). Tilly (1973) found that above a particle size of $100 \mu\text{m}$, the erosion ratio is independent of the particle size.

Particle density

In the same way the kinetic energy of a particle increases with size, the kinetic energy increases with density. As expected, the erosion rate increases with increasing particle material density. Because of the direct relation of the particle volume (size) and density with the impact energy, these parameters are important factors in determining the erosion rate.

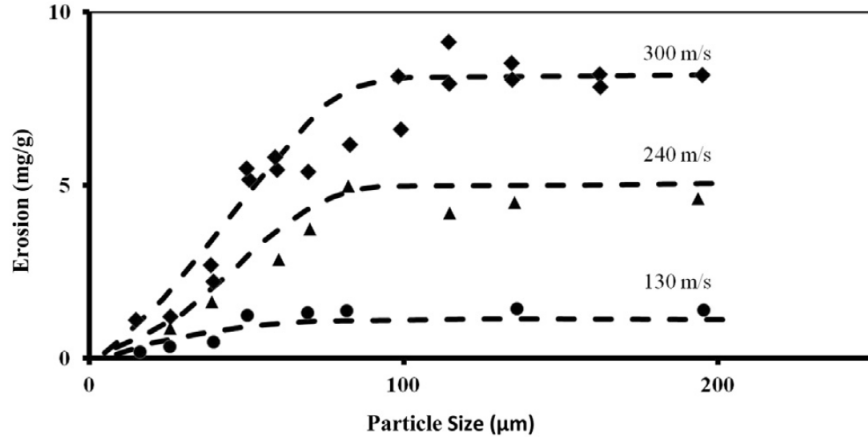


Figure 2.5: Erosion ratio versus particle size and particle impact velocity (Tilly, 1973)

Particle hardness

In general, the erosion rate will increase with increasing particle material hardness. This is especially true as long as the particle material hardness is smaller than the eroding material hardness. When the hardness of the particle material reaches a certain level, an increase of the hardness will not considerably increase the erosion rate. For AISI 1020 carbon steel, this is the case if the Vickers hardness of the particle rises above 700 HV (Parsi et al., 2014). A particle that is relatively soft in relation to the eroding material will shatter into pieces at the moment it hits the eroding surface. This reduces the kinetic energy and thus the erosion rate. Besides, the broken particle fragments cover the eroding surface, which also decreases the erosion rate (Levy and Chik, 1983).

Particle shape

The erosion rate is influenced a lot by the particle shape. Round spherical particles will cause a lower erosion rate than sharp angular particles (Finnie, 1960). Levy and Chik (1983) observed that the use of angular particles instead of spherical particles can result in an erosion rate that is four times higher.

Fluid (and particle) velocity

The flow velocity is one of the most influencing factors for the erosion rate, since it directly affects the impact velocity (and thus kinetic energy used for deformation) of the particles (Parsi et al., 2014). An interaction exists between the fluid and the impacting particles, as the flow applies a drag force to the particles. The velocity will be a fraction of the flow speed, depending on flow properties like density and viscosity.

A relation between the erosion rate and particle velocity can be written as:

$$\text{Erosion Rate} \propto V_L^n \quad (2.15)$$

In this equation, V_L is the impact velocity of the particle and n is a constant. Theoretical as well as experimental research has been done to determine the value for n . A value of 2 has been suggested by Finnie (1958) based on theoretical work. Laitone (1979a,b) suggested a value of 4. Other researches observed values for n ranging from 0.3 to 4.5 (Smeltzer et al., 1970; Burnett et al., 1995). Oka and Yoshida (2005) suggested in more recent research that n not a constant, but that it depends on the hardness of the eroded material.

Fluid viscosity and density

The properties of the carrier fluid determine the particle trajectory and speed. The direction and speed of the particles in the fluid is not by definition the same as that of the fluid itself (Finnie, 1960). As the fluid exerts a drag force on the particles, the particle velocity and thus impact velocity increase with increasing fluid velocity. Besides, when a relatively heavyweight particle travels in a low-viscosity fluid stream, it is less tended to follow the flow path. In this way, the fluid viscosity can affect particle velocity and impact angle. Even though some theories concerning the effect of fluid viscosity and density on the erosion rate are proposed, the relation is not fully understood yet (Parsi et al., 2014).

Eroded material hardness and toughness

Finnie (1967) states that the erosion resistance increases with increasing material hardness. However, observations done by Levy and Hickey (1981) indicate that materials with a high hardness show higher erosion rates than materials with a low hardness. The reason for this contradiction may be found in the different erosion mechanisms described in Paragraph 2.2. At a certain hardness level, the erosion mechanism changes from ductile erosion to brittle erosion. For this reason, it might be better to look for a correlation between the material toughness and the erosion rate. Increasing the material toughness means increasing the hardness of a material without the loss of ductility. In this case, a higher material toughness results in a lower erosion rate.

Eroded material ductility

The ductility of a material directly affects the energy required for plastic deformation of the surface. Craters and lips are formed more easily when a particle that hits a material with a relatively high ductility. When the ductile erosion mechanism is active, the erosion rate increases with increasing ductility. For the brittle erosion mechanism, the relation between eroding material ductility and erosion rate is not fully understood.

Eroded material strength

In general, an increasing eroding material strength results in a decreasing erosion rate. For a high-strength material, the hitting particle is more tended to break into pieces instead of cutting into the surface as one piece (Finnie, 1960).

Eroded area geometry

Irregular shapes and sudden geometry changes result in sudden changes in flow patterns and cause turbulent flows, which increase the erosion rate.

Particle concentration

Particle concentration can be defined in multiple ways. It is often defined as the weight or volume percentage of the particles in the carrying fluid. A more precise definition is the quantity of abrasive particles hitting a surface unit in a unit of time (g/cm^2) (Kleis and Kulu, 2007). With relatively small particle concentrations, the erosion rate is increasing linearly with increasing particle concentration, up to a certain point. Above this point other effects like particle-particle interactions occur and the relation is not linear anymore.

Temperature

Conflicting observations have been published on the effect of temperature on erosion rate. Smeltzer et al. (1970) state that the erosion rate decreases with increasing temperature. In a later research, Levy (1979) suggests that the erosion rate increases with increasing temperature. He states that increasing the temperature increases the ductility of the material, and thus the erosion rate increases. Even though the effect of temperature on erosion rate is not fully understood, agreement exists upon the fact that the influence is small (Parsi et al., 2014).

2.4 Erosion Rate Prediction Models

As discussed in the previous paragraphs, solid particle erosion is a complex phenomenon that is influenced by many factors. For this reason, predicting the erosion rate is a challenging task. Numerous scientific publications on this subject can be found in literature and a variety of models are proposed by researchers. However, the interrelatedness of all influencing factors is still not fully understood and no model has been developed yet that is capable of accurately predicting the erosion rate for multiple erosion circumstances and material combinations. However, models have been successful in describing erosion behavior in a qualitative manner.

Meng and Ludema (1995) published a review paper in which 28 erosion models proposed by literature (including 33 parameters) are reviewed. The conclusion was drawn that no general model is available for practical use, and that further research should focus of translating microscopic erosion observations to macroscopic models. About 20 years later, Parsi et al. (2014) used the review of Meng and Ludema (1995) as a basis and added some models that are proposed later. The current state of knowledge about the effect of several factors on the erosion rate was included in the paper as well. Besides, the principles of CFD and the application of this technique in erosion modelling is discussed. Although big improvements are made in erosion modelling in the last years, further research is required to overcome the following challenges (among others):

- Some aspects of the erosion phenomenon are still unknown. For instance, the effect of fluid viscosity on erosion is not fully understood.
- Finding a set of physical properties that is sufficient to develop a general erosion model
- Developing models for complex geometries. Current models are limited to simple geometries as tees and elbows
- Further research is required on the transition from brittle to ductile erosion and a way to implement this transition in erosion models should be developed

Chapter 3

Production Casing and Erosion Profiles

In this chapter, both the uneroded and the eroded production casings that are used for the FEA simulations are defined. In the first paragraph, the geometry of the uneroded casing is described. The material properties of the casing material can be found in Paragraph 3.2. Finally, in Paragraph 3.3 several erosion profiles are presented of which the effect on the external collapse pressure is evaluated in the next chapter.

3.1 Production Casing Geometry

Main dimensions

A uniform cross-section model is used to represent the production casing in the simulations. The average nominal outside diameter of the used model is 177.8 mm (7”), which is a commonly used tubing size for well completions (Bellarby, 2009). A wall thickness of 9.36 mm is used. Samples with the same dimensions are used by (Assanelli et al., 2000) to perform external pressure collapse experiments and casing collapse simulations. The main dimensions of the steel casing model are summarized in Table 3.1.

Average outside diameter d_o [mm]	177.8
Wall thickness t [mm]	9.36
Length L [mm]	1800

Table 3.1: Production casing model dimensions

Casing ovality

When producing the steel casings with the UOE production process, an ovality (imperfection) will be present in the range of 0.15% to 0.35% (Herynk et al., 2007). Assanelli et al. (2000) performed external pressure collapse experiments and used a measuring system to determine the ovality of the samples. An ovality of 0.18% turns out to be a common value, so this value is used in the simulations. The cross-section ovality is defined as:

$$Ov = \frac{d_{max} - d_{min}}{d_o} \quad (3.1)$$

In Figure 3.1, the cross-section of the steel casing is presented along with its dimensions. Note that the ‘vertical’ diameter is smaller than the ‘horizontal’ diameter, and thus an ovality is introduced.

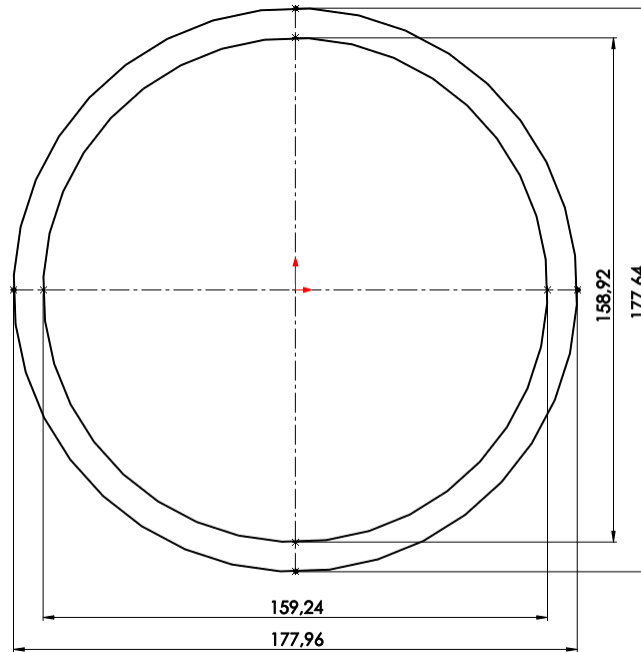


Figure 3.1: Production casing cross-section

Perforation tunnels

Perforation tunnels are present in the production casing to allow the fluid to flow from the production zone to the wellbore. The perforation tunnel configuration of a production casing can be defined by three parameters: tunnel diameter, shots per meter (SPM) and shot phasing. Phasing is defined as the angle between the perforation tunnels. The most common phasings are 0° , 60° , 90° , 120° and 180° , see Figure 3.2.

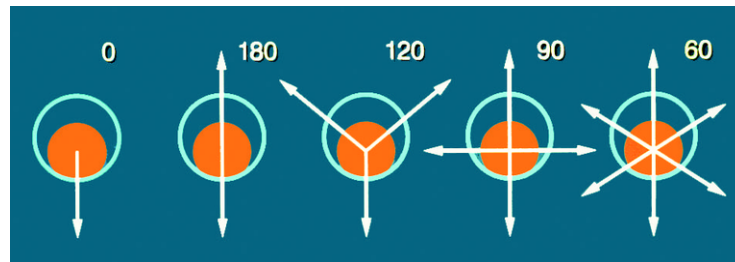


Figure 3.2: Commonly used gun phasings in perforation design (Petrowiki.org)

In the ideal situation that all perforations are open for flow, a shot density of 13 Shots Per Meter (SPM) with 13 mm ($1/2''$) diameter perforation tunnels, using a gun phasing of 90° results in the same production rate as an open well completion (Petrowiki.org). However, in reality

approximately 50% of the tunnels are producing fluid. For this reason, the shot density of the steel casing model is set to 26 SPM with a gun phasing of 90 degrees. The perforation design is summarized in Table 3.2.

Shots Per Meter (SPM)	26
Perforation tunnel diameter [mm]	13
Gun phasing	90 degrees

Table 3.2: Production casing perforation design

A side view of the production casing model is shown in Figure 3.3. In this figure it can be seen that the perforation tunnels are not located exactly opposite to each other, but are 'spiraling' on the casing surface. Each perforation tunnel is situated at a phase angle of 90 degrees with respect to the previous tunnel and $1/26 = 0.0038$ m further along the length of the casing.

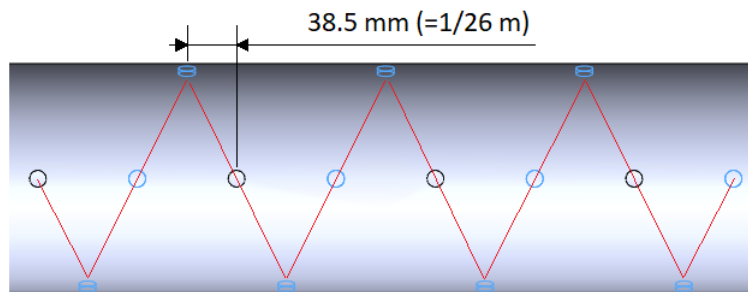


Figure 3.3: Perforation tunnels 'spiraling' around the casing surface

Furthermore, the charges used to create the perforation tunnels are not shot from the center of the casing (as can be seen in Figure 3.2). In Figure 3.4 a cross-section of the casing with the firing unit is shown.

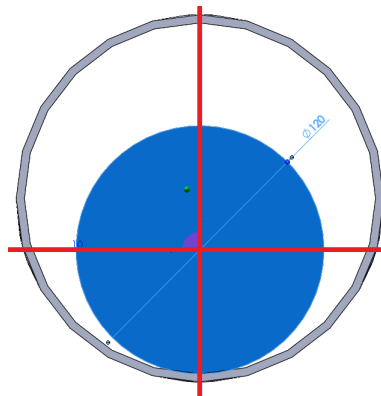


Figure 3.4: The penetration charges are fired from a decentralized position. The lines indicate the firing direction, and thus the position of the perforation tunnels

3.2 Production Casing Material Properties

The API defined a set of materials (steel grades) that can be used for the production of OCTG (Bull, 1985; Bourgoyne et al., 1991). The steel grades vary (among other properties) in yield strength, hardness and chemical resistance to sour environments. In designing the well, for each casing type it should be considered what the strength requirements are and thus which steel grade is suitable. As the production casing is the lowest part of the well, this casing is subjected to heavy loading conditions, both mechanically and thermally. For this reason, the higher steel grades are commonly used in this type of casing. As each well is different and multiple factors should be considered in the material choice, no ‘standard’ steel grade is present for each type of casing.

Grade L80 steel is used for the production casing models in this research. L80-grade steel is suitable for both sour and sweet service (Sovonex.com). The material properties relevant to this research are presented in Table 3.3. The minimum value given for the yield strength is used in both the API collapse strength calculations (Paragraph 2.1) and the FEA material models.

Young’s modulus [GPa]	206.8
Yield strength (min – max) [MPa]	552-665
Poisson ratio [-]	0.28

Table 3.3: Material properties of API grade L80 steel (Bellarby, 2009; Sovonex.com)

In Figure 3.5, the stress-strain graph of grade L80 steel is shown. In this graph, the true stress is plotted versus the true plastic strain. This data is used as input for the Multilinear Isotropic Hardening model (MISO) in the FEA models. This material model is described in Paragraph 4.1.

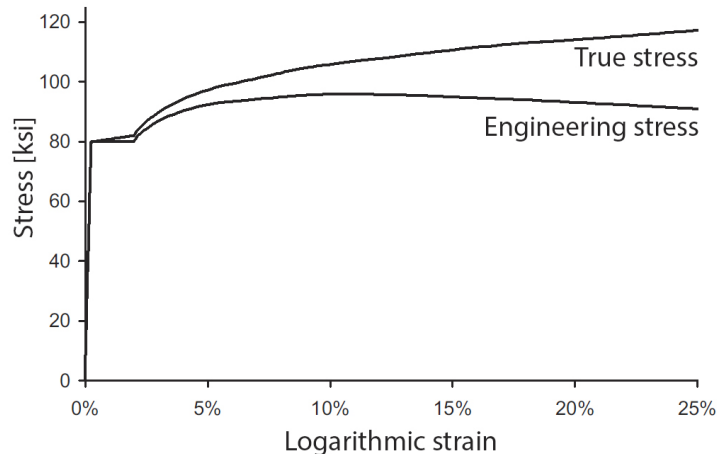


Figure 3.5: True stress vs. logarithmic strain of grade L80 steel (Klever et al., 2010)

3.3 Erosion Profiles

General approach

The next step is defining the erosion profile of the production casing geometry that is used to examine the effect of erosion on the external collapse pressure. In the ideal situation, a used and eroded specimen is taken from an oil/gas well and the exact erosion profile is measured. However, the common procedure for removing a steel casing from a well is milling it out. Removing (a part of) a production casing from the well without the specimen being broken is a very costly and uncommon operation. For this reason, other ways of determining the erosion profile should be considered. Other methods that can be used to calculate/determine the erosion profile are:

- Perform erosion experiments using the specific material – fluid system representing the well conditions. In the experiments, flow parameters that are dominating the erosion rate (like impact velocity and attack angle, see Paragraph 2.3) should be varied. The experimental data can be fit to an empirical model that describes the erosion rate under varying flow properties. The second step is using Computational Fluid Dynamics (CFD) to simulate the flow in the production casing. Combining the obtained erosion model with the calculated flow in an FEA simulation, the erosion profile can be calculated.
- Use a (semi-)analytical erosion model proposed in literature to represent the erosion behavior. Calculate the flow properties using CFD analysis and combine the CFD results with the erosion model in an FEA simulation to calculate the erosion profile.
- Evaluate the geometry of the production casing and assume a flow path and erosion profile based on a general understanding of the erosion phenomenon and flow behavior.

The abovementioned methods for determining the erosion profile are listed from the most accurate/scientific approach to the least one. In the first and second option, CFD simulations are used to determine the flow properties. This is not an easy/straightforward simulation; calculating the flow properties in a production casing is a project on itself. Unfortunately, the available time for this research is insufficient to include this simulation. This also accounts for the erosion experiments. Another drawback of the first two methods is that the erosion profile that is calculated cannot be validated using field specimen of the casing. As mentioned in Paragraph 2.3, erosion is a complex phenomenon, affected by numerous parameters. For this reason, researchers have not succeeded in formulating models that are capable of accurately predicting the erosion rate. However, researchers succeeded in using erosion models to examine the effects of flow and material parameters in a qualitative manner.

As the requirements of the first and second method do not fit to the extent of this research, the third method is applied. Although this is not the most scientific approach among the available options, using this method is effective when applied in a good manner. In the remaining of this paragraph, multiple erosion profiles are described. The advantage of using multiple erosion profiles is that the effect of specific characteristics of the erosion profile on the external collapse pressure value can be evaluated. In this way, the nature of the research is more qualitative than quantitative.

Defining erosion profile

Because the perforation tunnels are shot decentralized, two types of flow paths are present. One flow path hits the surface with a 90 degrees (normal) angle and one flow path hits the casing surface with an angle smaller than 90 degrees. This is clarified in Figure 3.6. The total erosion profile is specified by three areas:

- Area 1: Increased perforation tunnel diameter
- Area 2: Decreased wall thickness (90 degrees flow angle relative to wall surface)
- Area 3: Decreased wall thickness (<90 degrees flow angle relative to wall surface)

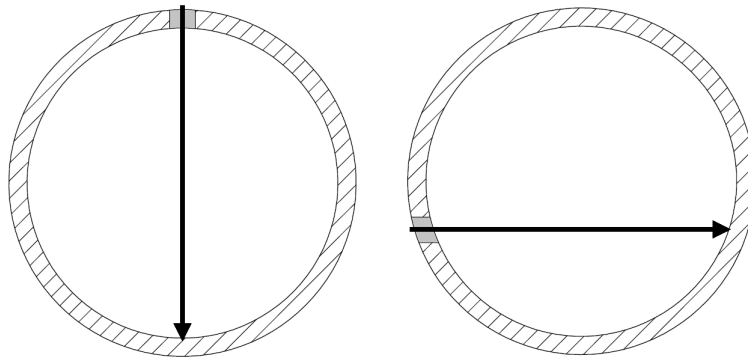


Figure 3.6: The oil/gas flow hits the surface with a normal impact angle at erosion area 2 (left) and with an angle <90 degrees at erosion area 3 (right)

Erosion profile area 1

The first erosion profile is relatively simple and can be described by an increased perforation tunnel diameter.

Erosion profile area 2

In this erosion area, the oil/gas flow hits the casing surface directly opposite to the perforation tunnel with an impact angle of 90 degrees (normal impact). The erosion rate is at its maximum at the center of the flow hitting the surface. The erosion profile is split up in two parts (see Figure 3.7):

- Projected area of perforation tunnel onto casing surface: uniform wall thickness decrease
- Circle surrounding the projected area, with a diameter of three times the perforation tunnel diameter: erosion profile decreases linearly to zero

Erosion profile area 3

In this area the flow hits the surface at an angle smaller than 90 degrees, so the erosion profile is not symmetric. The erosion profile is split in two parts again (see Figure 3.8):

- Projected area of perforation tunnel onto casing surface: uniform wall thickness decrease
- Area at one side of the perforation tunnel projection with a length of two times the tunnel diameter: erosion profile decreases linearly to zero.

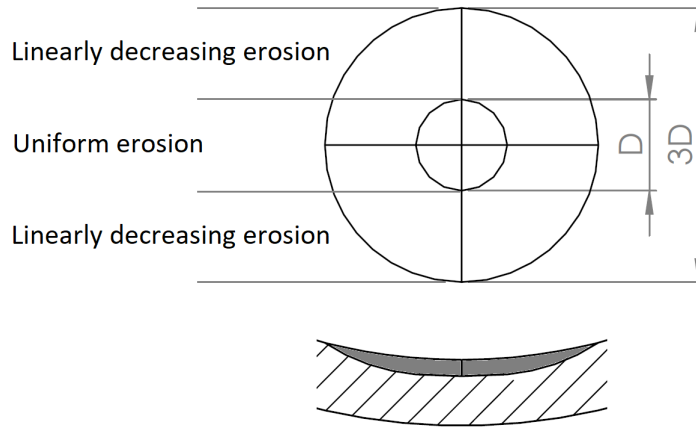


Figure 3.7: Erosion profile of area 2 (normal incidence angle)

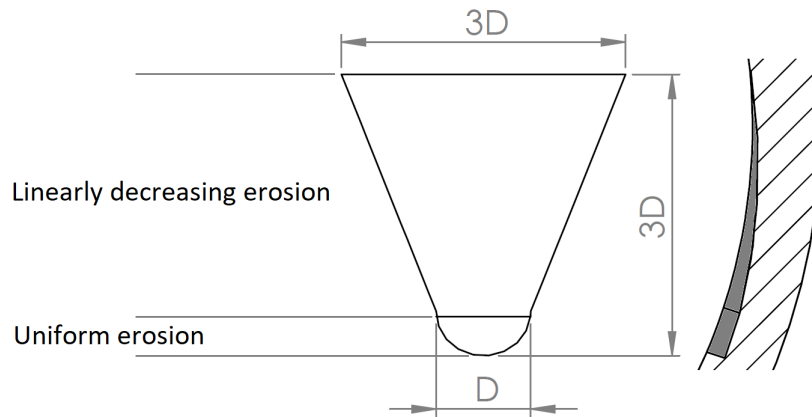


Figure 3.8: Erosion profile of area 3 (normal incidence angle)

Evaluated erosion models

Figure 3.9 gives a 3D impression of the erosion profiles described above. In order to distinctly evaluate the effect of the wall thickness decrease and the perforation tunnel increase, multiple erosion profiles are evaluated. An overview of these models is given in Table 3.4.

Erosion model no.	Wall thickness	Tunnel diameter
1	Maximum decrease of 10%	Increase of 10%
2	Maximum decrease of 10%	No increase
3	No decrease	Increase of 10%
4	Maximum decrease of 25%	Increase of 25%
5	Maximum decrease of 25%	No increase
6	No decrease	Increase of 25%

Table 3.4: Overview of erosion models used in simulations

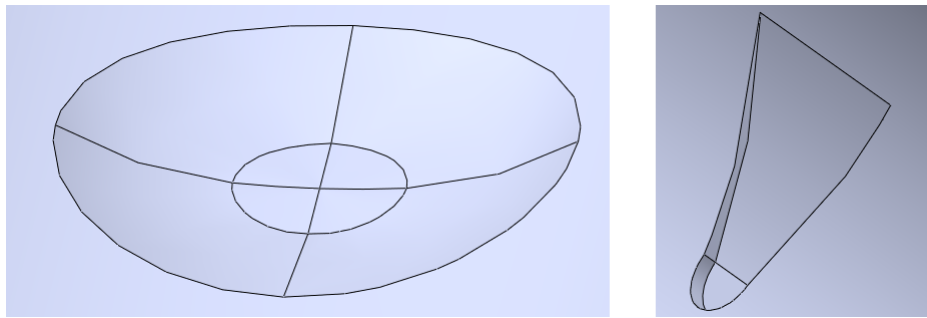


Figure 3.9: Left: erosion area 2, right: erosion area 3

Chapter 4

Collapse Simulations

Based on the information gathered in the previous chapters, FEA simulations are done. The results of these simulations are presented in this chapter. In the first paragraph, the basic configurations and properties of the FEA models are discussed. In the second paragraph, the validity of the models is discussed. Finally, the results of the external collapse pressure simulations of the uneroded and eroded production casing are presented.

4.1 FEA Model Description

The basic FEA model configurations and properties will be discussed in this section. As a result of the model validation section (Paragraph 4.2), an ‘ideal’ model configuration will be given. This model configuration will be used in the collapse simulations of the steel casing (Paragraph 4.3). All simulations are performed with ANSYS Workbench.

Boundary conditions and loads

For the model validation simulations, half of the pipe is modeled and a symmetry region is defined in ANSYS. This reduces the calculation cost of the simulation, while obtaining similar results. In the experimental setup used for external collapse tests the steel casing is fixed at both ends, so in the model a fixed support boundary condition is imposed on the casing end. An overview of the boundary conditions is depicted in Figure 4.1. Note that the symmetry region is only used for the model validation simulations. Because of the ‘spiraling’ perforation tunnels, the production casings have no symmetry plane(s).

Model geometry

The geometry of the production casing used for the simulations is described in Chapter 3. For the model validation part, the geometry of a production casing is used, without the presence of the perforation tunnels. To make sure that the fixed support boundary conditions at the end of the pipe do not affect the collapse behavior at the midpoint of the pipe, the L/D ratio is ensured to be bigger than 10.

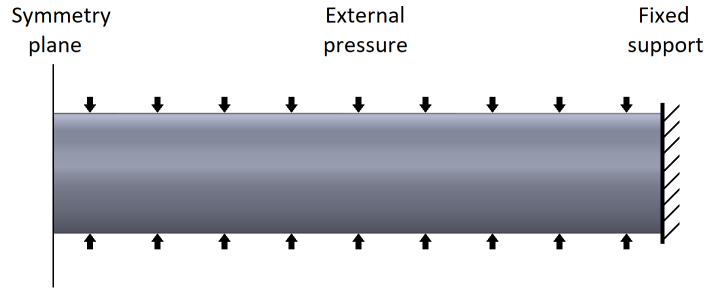


Figure 4.1: Boundary conditions

Element type

The element used in the simulations is the *Solid187* element. This is a three dimensional element with quadratic displacement behavior (see Figure 4.2). The element is capable of dealing with irregular meshes and furthermore can deal with plasticity, hyperelasticity, creep, stress stiffening, large deflections and large strain. For abovementioned reasons, the element is suitable for the collapse simulations.

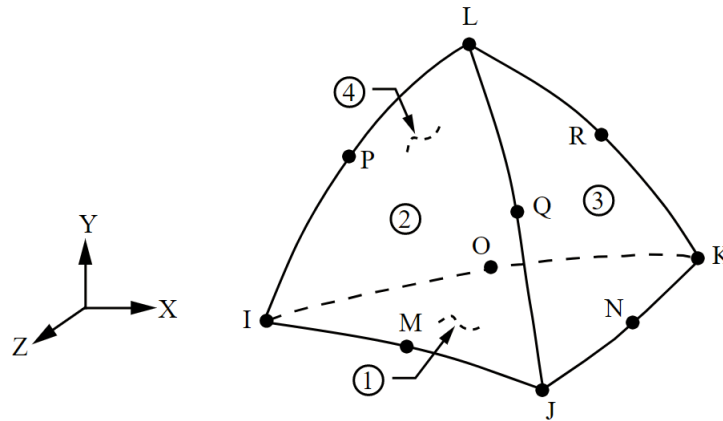


Figure 4.2: Solid187 element (Sharcnet.ca)

Meshing

In determining the element size, a balance is sought between calculation cost and result accuracy. Furthermore, a mesh that is too coarse will lead to big mesh distortions and thus a non-converging model. The first step is finding the maximum element size for which the model converges and the element distortion is acceptable. Secondly, the element size is decreased until no significant changes in the simulation results is observed. The effect of mesh refinement at specific areas is evaluated. Simulations are run with mesh refinements at the perforation tunnels and the decreasing wall thickness erosion profiles (see Figure 4.3). The refinement dramatically increases the calculation cost, while no significant change in results is observed. For this reason, no mesh refinement is applied in the model validation and production casing collapse simulations.

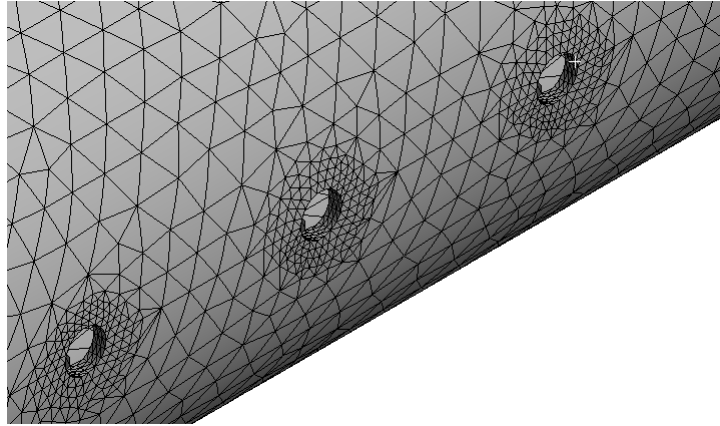


Figure 4.3: Factor 2 mesh refinement applied around the perforation tunnels

Material models

The material properties of grade L80 steel are presented in Chapter 3. For the model validation, two different material models are used:

- Bilinear Isotropic Hardening Model (BISO)
- Multilinear Isotropic Hardening Model (MISO)

A BISO model is often used for large strain analyses. The input values for this model are the Young's modulus for the elastic region, the yield stress and a tangential modulus for the plastic region. The model is defined by using nominal stress and strain. However, as the 'Large deflection' option is activated in the simulations, ANSYS accounts for the change of cross section areas due to large deflections and uses the true plastic stain and true stress for the calculations. A graphical presentation of the input data for the BISO model is shown in Figure 4.4.

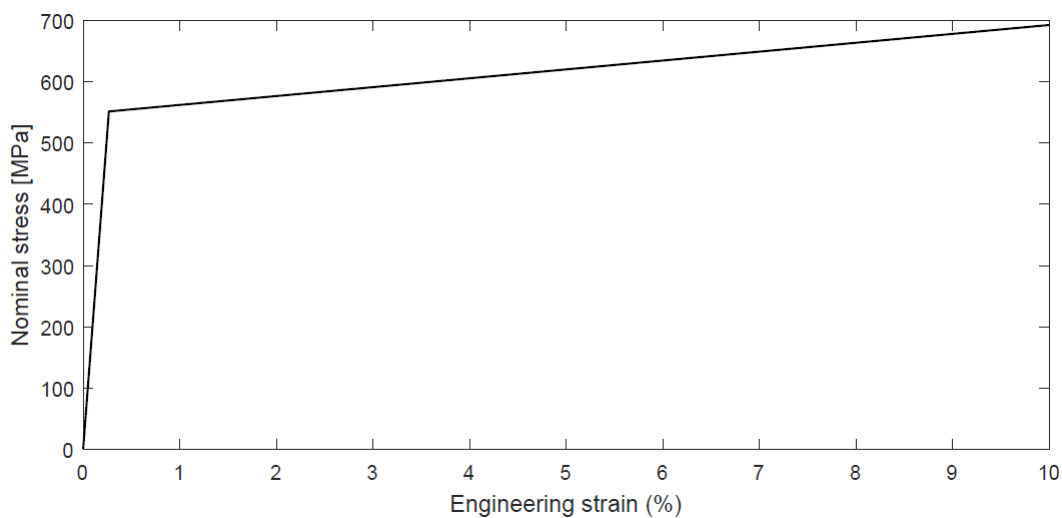


Figure 4.4: Input for the BISO material model

The MISO model can be used if more information about the plastic behavior is known. For the plastic region, the stress-strain curve consists of several segments with different tangential moduli. True plastic strain – true stress data points of the stress-strain curve are used as input for the MISO model. The true plastic strain and the true stress can be calculated (using the engineering strain and nominal stress) by:

$$\epsilon_{true} = \ln(1 + \epsilon_{eng}) \quad (4.1)$$

$$\sigma_{true} = \sigma_{eng}(1 + \epsilon_{eng}) \quad (4.2)$$

A graph of the MISO material model is shown in Figure 4.5. The first point of the curve corresponds to the true stress and yield and the true plastic strain at yield (which is zero). This point defines the slope of the linear region of the stress-strain curve, and thus the linear response of the material.

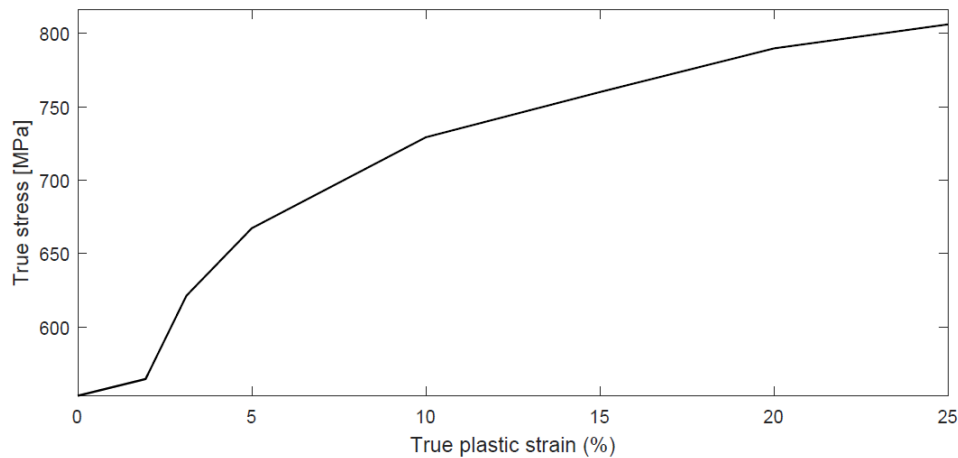


Figure 4.5: Input for the MISO material model

Nonlinear analysis settings

The following nonlinear analysis settings are used:

- Large deflection: on
ANSYS recalculates the stiffness matrix as the structure deflects.
- Nonlinear stabilization control: on (energy controlled)
In a collapse simulation, the structure becomes unstable when the load reaches a certain value. In order to avoid convergence problems, the stabilization control technique is used. This can be seen as applying artificial dampers/dashpots to the nodes. The dampers are fixed to the ground and ANSYS calculates a damping force that is proportional to the velocity of the nodes (displacement increment divided by the time increment of substep). An Energy Dissipation Ration (EDR) is used as input, with a value between 0 and 1. A higher EDR value results in higher damping forces.
- Time stepping: 100
For convergence reasons, the external pressure is applied in 100 time steps.

4.2 Model Validation

In this section, the results of collapse simulations of three casing geometries are compared to analytically calculated collapse pressures. In this way it is evaluated whether the FEA models are capable of predicting the actual collapse pressure.

Main approach and models

Three (unperforated) steel casing models are used for the purpose of FEA model validation. The dimensions of these models are given in Table 4.1. The equations given by the American Petroleum Institute (see Paragraph 2.1) are used to analytically determine the collapse pressure of the casings. Several simulations will be run for each geometry to find out the effect of changing certain simulation parameters. The collapse pressures found by the simulations are compared to the analytically determined pressures and a conclusion is drawn about the validity and usability of the model.

	Model 1	Model 2	Model 3
Outside diameter [mm]	244.5 (9 5/8")	177.8 (7")	177.8 (7")
Wall thickness [mm]	14.64	7.83	9.36
D/t ratio	16.7	22.7	19.0
Ovality (%)	0.18	0.18	0.18
API collapse pressure [MPa]	64.6	37.8	52.4

Table 4.1: Validation models dimensions and API collapse pressures

Simulation configurations and results

Most simulation parameters will be held constant for each simulation, these parameters are described in Paragraph 4.1. However, the material model and the value for the Energy Dissipation Ratio (EDR) will be varied to evaluate the effect on the results. The EDR is an input value that is required since the *Nonlinear Stabilization Control* option is activated (see Paragraph 4.1). The used material models are described earlier in this chapter.

An overview of the simulation configurations and the main results can be found in Table 4.2. Note that the maximum displacement, maximum strain and maximum stress are insignificant results. The applied external pressure in each simulation is just above the collapse pressure, so the deformation, strain and stress results give information about the post collapse behavior. However, these results are included to evaluate the effect of changing simulation configurations (material model and EDR value).

Method for determining FEA collapse pressure

In order to make a fair comparison between the results of the different simulations, a method is defined to determine the collapse pressure. The instant that the casing starts to collapse can be recognized by a relatively large displacement increase (at the collapse region) caused by a small increase in the external pressure. As can be seen in Figure 4.7, the collapse starts at the center at the casing, so the displacement will always be at maximum at this location. Note that Figure 4.7 displays the deformation at an external pressure above the collapse pressure.

Model – Sim.	M1-S1	M2-S1	M2-S2	M3-S1	M3-S2	M3-S3	M3-S4
Material model	MISO	MISO	BISO	MISO	BISO	MISO	MISO
EDR [-]	0.5	0.5	0.5	0.5	0.5	0.25	0.75
No. of elements	33,952	31,107	31,107	38,116	38,116	38,116	38,116
No. of nodes	62,504	64,882	64,882	71,364	71,364	71,364	71,364

u_{max} [mm]	5.45	28.94	29.28	2.27	2.08	8,79	1.31
ϵ_{max} (%)	0.34	0.40	0.51	0.36	0.36	0.37	0.36
σ_{max} [MPa]	650.6	651.1	651.1	590.9	590.9	593.0	588.8
$P_{CO,FEA}$ [MPa]	79.8	57.4	57.2	69.5	69.3	68.6	70.0
$P_{CO,FEA}/P_{CO,API}$ [-]	1.23	1.52	1.51	1.33	1.32	1.31	1.34

Table 4.2: Simulation configurations and main results

The FEA collapse pressure $P_{co,FEA}$ is determined by evaluating the size of the deformation increments per pressure increment. In Figure 4.6, an external pressure versus maximum total displacement plot is shown. It can be observed from this plot that the maximum displacement will increase (approximately) linearly up to a certain external pressure limit. From this point, a small increase in the external pressure causes a relatively large increase in the total displacement. For each simulation the external pressure is applied in 100 equally sized steps, so the collapse pressure can be found by evaluating the size of the displacement increments. The relative change in displacement increment size at time step t is calculated with:

$$\text{Relative displacement increment size change} = \left| \frac{u_{max}(t) - u_{max}(t-1)}{u_{max}(t-1)} \right| * 100\% \quad (4.3)$$

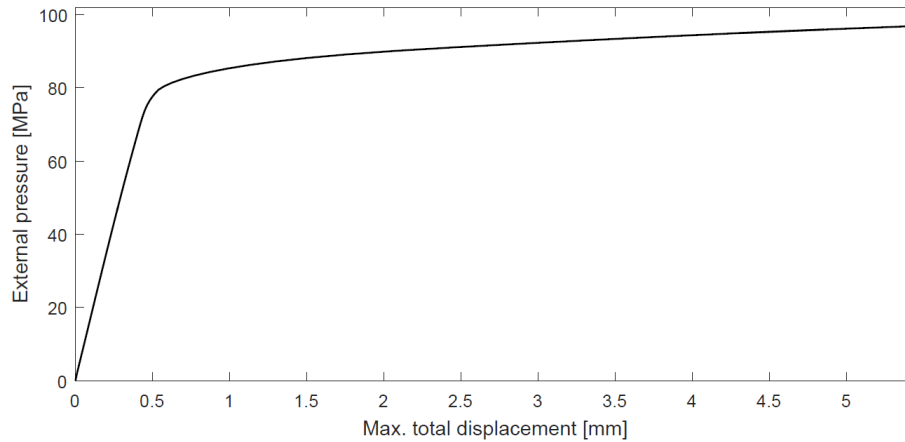


Figure 4.6: Maximum total deformation vs. external pressure (M1-S1)

In Figure 4.8, the external pressure is plotted versus the relative change in displacement increment size. *The FEA collapse pressure is defined as the pressure at which the relative displacement increment change is equal to 5 percent.*

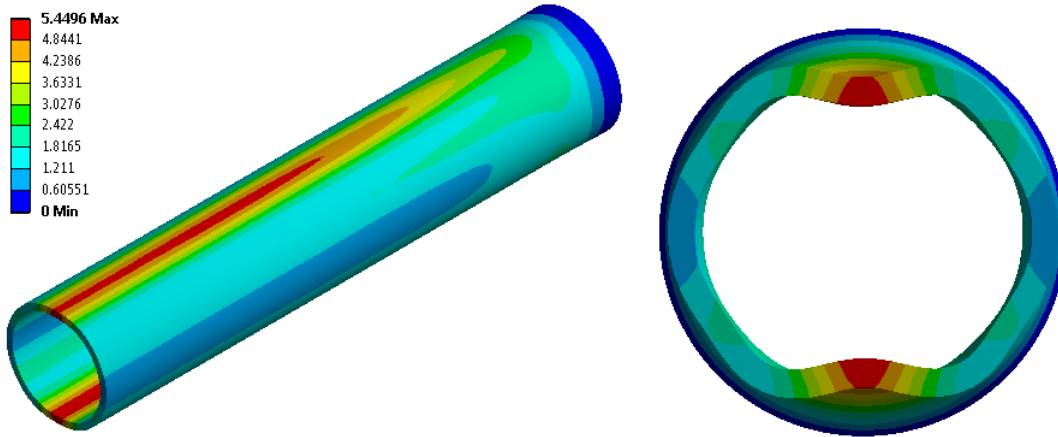


Figure 4.7: Maximum total deformation of M1-S1 (left: true scale, right: 5.9x)

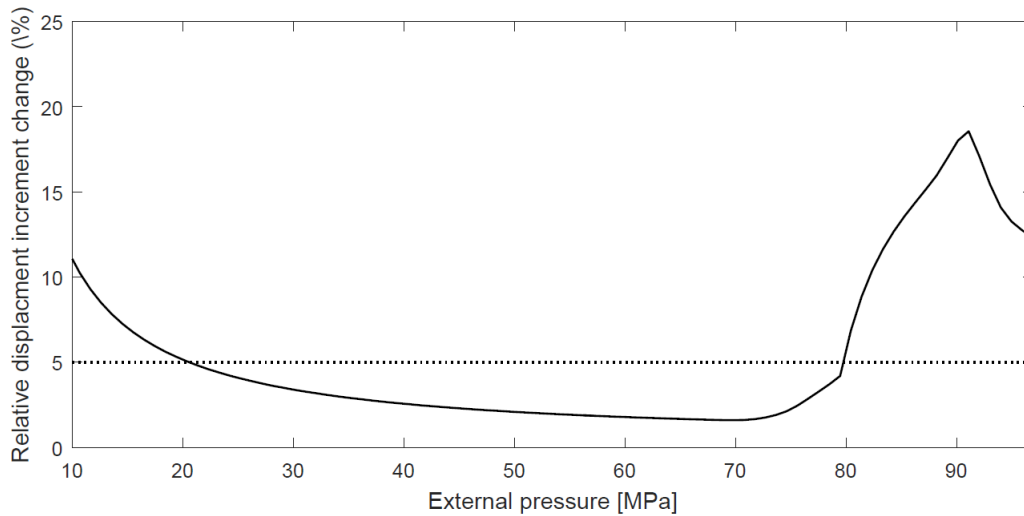


Figure 4.8: External pressure vs. relative displacement increment change (M1-S1)

Effect of material model

For each geometry, simulations are done with both the MISO and the BISO material model (see Paragraph 4.1). No significant differences are observed for the maximum total deformation, maximum equivalent strain, maximum equivalent stress and the collapse pressure. As the collapse pressure is the most important result and no difference is observed between both material models, it can be concluded that both models are suitable for this purpose.

Effect of energy dissipation ratio

For model 3, simulations are done with an energy dissipation ratio of 0.25 (M3-S3) and 0.75 (M3-S4). While the difference for the total deformation is significant (M3-S3: 8.79 mm; M3-S4: 1.31 mm), the difference between the collapse pressures is considered insignificant (M3-S3: 68.6 MPa; M3-S4: 70.0 MPa). This means that the energy dissipation ratio mainly affects the post-collapse behavior.

Configuration for further simulations

The value for the collapse pressure determined by the simulations is not significantly affected by the choice of material model and the value that is used for the energy dissipation ratio. However, the MISO material model is better capable in predicting the real stress state. For this reason, the MISO material model will be used for the remaining simulations in this chapter. An Energy Dissipation Ratio of 0.5 will be used.

Although the collapse pressure is structurally overestimated by the FEA simulations, it is assumed that the effect of erosion on the external collapse pressure can be evaluated using the simulations. In Chapter 6, possible causes for the overestimation of the collapse pressure are discussed.

4.3 Production Casing Collapse Simulations

The collapse simulation results of the uneroded and eroded production casing models are presented in this paragraph. The configurations used in the simulations are discussed in Paragraph 4.1 and Paragraph 4.2. The MISO material model and an EDR of 0.5 are used. The erosion profiles mentioned in the table are described in Paragraph 3.3. The simulation results are presented in Table 4.3. Figure 4.9 shows the total deformation of the production casing with erosion profile 1. Note that this figure shows the post-buckling behavior of the casing.

	Max. erosion profile depth	No. of elements	No. of nodes	$P_{co,FEA}$	Collapse ratio
Uneroded	0%	76,070	142,955	63.9	1
Profile 1	10%	80,400	150,278	60.7	0.95
Profile 2	10%	76,032	144,846	62.0	0.97
Profile 3	10%	74,990	141,318	62.7	0.98
Profile 4	25%	78,654	147,855	56.7	0.89
Profile 5	25%	78,622	147,986	59.6	0.93
Profile 6	25%	75,398	141,752	60.8	0.95

Table 4.3: Results of uneroded and eroded production casing collapse simulations

To evaluate the effect of the erosion profiles on the collapse pressure, the collapse pressure ($P_{co,FEA}$) is compared to the collapse pressure of the uneroded production casing. The collapse ratio is defined as follows:

$$\text{Collapse ratio} = \frac{P_{co,FEA}}{P_{co,FEA}(\text{Uneroded})} \quad (4.4)$$

The largest decrease in FEA collapse pressure is observed for erosion profile 1 and 4. These results are like expected, because these profiles contain both a decreased wall thickness and a decreased perforation tunnel diameter. Furthermore, the separate effects of a decreased wall thickness (profile 2 and 5) and an increased perforation tunnel diameter (profile 3 and 6) is evaluated. It can be concluded that the effect of decreased wall thickness on the external collapse pressure is bigger than the effect of the increased tunnel diameter.

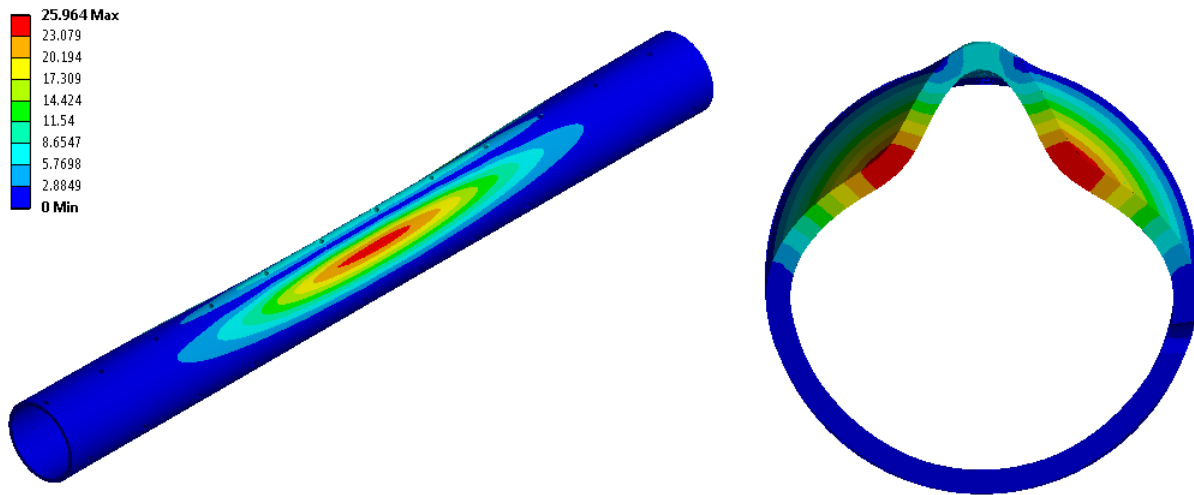


Figure 4.9: Total deformation of production casing with erosion profile 1 (true scale)

Chapter 5

Conclusions

The collapse pressure of a common steel casing can be calculated with the *Shell Collapse Pressure Equation* or using the *API Collapse Pressure Formulas*. The API formulas are considered most accurate and are also used in common practice for well design.

Particle material, angle of impingement, particle impact velocity and particle size determine which erosion mechanism is active. In addition to these factors, there are other factors that influence the erosion rate, of which a list is provided and the effect of each factor on the erosion rate is discussed. No general erosion prediction model is present in literature that is suitable for practical use. This is because some aspects of the erosion mechanism are not fully understood yet and further research is required to develop a consistent set of physical parameters that can describe the erosion situation.

Simulations are done with common steel casing geometries (without the perforation tunnels) to examine the validity of the FEA model. The FEA collapse pressure is compared with the API collapse pressure. Three steel casing geometries are used for model validation, which resulted in FEA collapse pressure over API collapse pressure ratios of 1.23, 1.52 and 1.33.

The effect of the erosion profiles on the external collapse pressure is evaluated by comparing the FEA collapse pressure to the FEA collapse pressure of the uneroded casing. As expected, the erosion profiles with both the wall thickness decrease and the tunnel diameter increase show the largest drop in collapse pressure (decrease of 5% for the 10% profile and 11% for the 25% profile). Furthermore, it can be concluded that the effect of decreased wall thickness on the external collapse pressure is bigger than the effect of the increased tunnel diameter.

Chapter 6

Discussion and Recommendation

The main results of the model validation simulations and the uneroded and eroded production casing collapse simulations are presented in Table 6.1. The FEA collapse pressures determined with the model validation simulations are structurally higher than the calculated API collapse pressures. The possible reasons for this difference, along with recommendations for further research, are discussed in this chapter.

Model validation simulations	$P_{co,FEA} / P_{co,API}$
Model 1 - Simulation 1 (MISO, EDR = 0.5)	1.23
Model 2 - Simulation 1 (MISO, EDR = 0.5)	1.52
Model 2 - Simulation 2 (BISO, EDR = 0.5)	1.51
Model 3 - Simulation 1 (MISO, EDR = 0.5)	1.33
Model 3 - Simulation 2 (BISO, EDR = 0.5)	1.32
Model 3 - Simulation 3 (MISO, EDR = 0.25)	1.31
Model 3 - Simulation 4 (MISO, EDR = 0.75)	1.34
Production casing collapse simulations	$P_{co,FEA} / P_{co,FEA} \text{ (Uneroded)}$
Uneroded	1
Profile 1 (max. 10%, wall thickness + tunnel diameter)	0.95
Profile 2 (max. 10%, wall thickness only)	0.97
Profile 3 (max. 10%, tunnel diameter only)	0.98
Profile 4 (max. 25%, wall thickness + tunnel diameter)	0.89
Profile 5 (max. 25%, wall thickness only)	0.93
Profile 6 (max. 25%, wall thickness + tunnel diameter)	0.95

Table 6.1: Results model validation simulations and production casing collapse simulations

Model geometry and erosion profiles

The ovality of the circular cross-section of the steel casings is the only imperfection that is incorporated in the models. However, in reality there are other imperfections present such as eccentricity and material imperfections. Besides, the ovality is modeled as a constant along the length of the casing, as it will be varying along the length of the casing in reality. Measuring imperfections like ovality, eccentricity and material imperfections and incorporating them in the model would probably increase the accuracy of the results. Assanelli et al. (2000) follow this

approach and use several measurement instruments to measure imperfections of the samples used in collapse pressure experiments. The results of their FEA simulations is in close agreement with the collapse experiment results.

The erosion profiles used in the simulations are 'assumed' erosion profiles. The geometry of the production casing is analyzed and the flow path and resulting erosion profile are assumed based on a general understanding of flow behavior and erosion. Assuming that the shape of the erosion profile is close to reality, this approach makes it possible to study the general effect of erosion on the structural integrity of the casing. To improve the accuracy of the simulation results, other techniques can be used to predict the erosion profile in further research. As suggested in Chapter 3, CFD analysis can be used to predict the flow path of the oil/gas entering the production casing. As a subsequent step, the results of erosion experiments can be combined with the CFD simulations outcome to more accurately predict the erosion profile.

In this study, the effect of erosion on external collapse pressure is examined for only one production casing type. In further research, it can be examined whether the results of this research are also valid for production casings with other geometries (diameter, wall thickness, gun phasing angle, shots per meter, perforation tunnel diameter) and materials.

Effect of residual stress

The UOE production process results in a steel casing in which internal residual stresses are present. Assanelli et al. (2000) use the 'slit ring test' to examine the amount of residual stress present in the samples. In this test, a small section ($L/D \approx 1$) is removed from the sample. The piece is cut open, and as a result of the residual stresses a gap is formed. By measuring the resulting gap, the amount of internal residual stress is calculated. Assanelli et al. (2000) observe that the presence of residual internal stresses causes a decrease in external collapse pressure of up to 30%. The residual stresses are not included in the FEA models, so this could be the main reason that the FEA collapse pressures are structurally higher than the API collapse pressures.

Validity of boundary conditions

In the FEA model, fixed boundary conditions are modeled at the casing ends. However, in reality these fixed boundary conditions are not present, as the casing ends are capable of radial expansion/compression. Ideally, the casing should be modelled as an infinite pipe to be sure the fixed boundary condition has no effect on the collapse pressure. However, due to limited calculation capacity the maximum casing length is restricted. The assumption is made that a minimum L/D ratio of 10 is sufficient to eliminate the effect of the fixed boundary condition. No simulations are done with bigger L/D ratios, so the result of increasing the L/D ratio could be examined in further research.

Besides the fixed support boundary conditions at the casing ends, an external pressure is exposed on the outer casing surface. This is a relatively simple load situation. In the real situation, there are some other factors that influence the collapse pressure. For instance, an internal pressure is present as well. Besides, the cementing job could influence the structural integrity. As the goal of this research is only to examine the effect of erosion on the collapse pressure, it is assumed that the simple load system that is used is sufficient to examine this effect.

Method of collapse pressure determination

As described in Paragraph 4.2, the FEA collapse pressure is defined as the pressure at which the relative displacement increment change is equal to 5%. Even though this method provides the possibility to accurately determine a collapse pressure for each simulation and thus make a fair comparison between the results of the simulations, the '5% threshold assumption' is based on common sense. In further research the validity of this method could be evaluated in order to improve the results.

Nonlinear analysis settings

For convergence reasons, the 'nonlinear stabilization' option is activated in the simulations (see Paragraph 4.2). The EDR value, which is required as input for this option, should lie in the range of 0 to 1. It is observed that varying the EDR value has no significant effect on the calculated FEA collapse pressure. For this reason, an EDR value of 0.5 is used in all simulations. However, the EDR value does significantly effect the post collapse behavior, so when this behavior is studied in further research, attention should be given to this input value.

As the 'program controlled' time stepping option causes convergence problems, the number of time steps is set manually to 100 in all simulations. The external pressure is applied linearly, so the pressure increment is equal for each time step. Simulations are run with few and more than 100 time steps to find the optimal balance between result accuracy and calculation cost. To decrease the calculation cost, applying the external pressure can be split up in two parts. During the first part, few time steps can be used to apply the pressure while deformation is still in the elastic region. For the second (nonlinear) part, smaller time steps can be used.

Material models

Two material models are used in the model validation simulations. For the MISO model, true plastic strain vs. true stress (experimental) data is required, while for the BISO model only the Young's modulus, yield strength and a tangential modulus for the tangential region is required as input. Even though the MISO model is better capable of representing the real material behavior, no significant differences are observed in the results for both material models. This means that the knowledge of basic material properties is sufficient to accurately predict the collapse pressure, and other materials can be used in future research.

Recommendations for further research

The validity of the assumptions and methods of this research are discussed in this chapter. In short, the recommendations for further research that are mentioned above are:

- Use other production casing geometries (dimensions, perforation design)
- Examine validity of method for collapse pressure determination or use other method
- Use CFD simulations in combination with erosion experiments to more accurately predict the erosion profile
- Include residual stresses in FEA model
- Examine the result of the L/D ratio on the collapse pressure

Appendix A

Hosting organization and role

Institut Teknologi Bandung

Founded in 1920, Institut Teknologi Bandung (abbreviated by ITB) is the oldest technological university of Indonesia. It is one of the three big technical universities of Indonesia and is situated in Bandung, which is about 160 km from Jakarta. The current president of Indonesia, Soekarno, finished his architecture degree at this university and for most students this university is the first choice.

My role in the organization

During my internship I was part of the Mechanical Engineering and Aerospace Engineering Faculty (Fakultas Teknik Mesin dan Dirgantara), at a specific laboratory of Mechanical Engineering. My supervisor, Bagus Budiwantoro, is head of this laboratory. He arranged a student of the department to pick me up from my arrival point in Bandung. I had a very warm welcome and this student, Ken Kartawijaya, showed me my apartment, helped me arranging practical matters and showed me around in Bandung during the first week.

At my first arrival at ITB, I had a warm welcome of Mr. Bagus and a colleague professor (Rachman Setiawan). I discussed the goal of my research with Mr. Bagus and he set up a meeting in the same week with a visiting professor from Jakarta to discuss about my subject. Besides, I made a planning for my research in the second week, that was approved by Mr. Bagus and Mr. Rachman. In the second week I also gave a presentation about the University of Twente for the staff of the department and some master students. For the remaining of my research, I updated my progress to Mr. Bagus and Mr. Rachman either by presenting it to them or by email. For the simulations I needed to perform for my research, I made use of the desktop PC that was available at the laboratory.

Bibliography

- Assanelli, A. P., Toscano, R. G., Johnson, D. H., and Dvorkin, E. N. (2000). Experimental/numerical analysis of the collapse behavior of steel pipes. *Engineering computations*, 17(4):459–486.
- Bellarby, J. (2009). *Well completion design*, volume 56. Elsevier.
- Bourgoyne, A. T., Millheim, K. K., Chenevert, M. E., and Young, F. S. (1991). *Applied drilling engineering*, volume 2. Society of Petroleum Engineers Richardson, TX.
- Bull, A. (1985). 5c3. *Bulletin for Formulas and Calculations for Casing, Tubing, Drillpipe, and Line Pipe Properties*,.
- Burnett, A., De Silva, S., and Reed, A. R. (1995). Comparisons between “sand blast” and “centripetal effect accelerator” type erosion testers. *Wear*, 186:168–178.
- Clark, H. M. (1991). On the impact rate and impact energy of particles in a slurry pot erosion tester. *Wear*, 147(1):165–183.
- Desale, G. R., Gandhi, B. K., and Jain, S. (2009). Particle size effects on the slurry erosion of aluminium alloy (aa 6063). *Wear*, 266(11):1066–1071.
- Dvorkin, E. N. and Toscano, R. G. (2003). Finite element models in the steel industry: Part ii: Analyses of tubular products performance. *Computers & Structures*, 81(8):575–594.
- Elkholy, A. (1983). Prediction of abrasion wear for slurry pump materials. *Wear*, 84(1):39–49.
- Finnie, I. (1958). The mechanism of erosion of ductile metals. In *3rd US national congress of applied mechanics*.
- Finnie, I. (1960). Erosion of surfaces by solid particles. *wear*, 3(2):87–103.
- Finnie, I. (1967). Erosion of metals by solid particles. *J. of Materials*, 2(3):682.
- Gandhi, B. and Borse, S. (2002). Effects of particle size and size distribution on estimating erosion wear of cast iron in sand-water slurries.
- Herynk, M., Kyriakides, S., Onoufriou, A., and Yun, H. (2007). Effects of the uoe/uoc pipe manufacturing processes on pipe collapse pressure. *International Journal of Mechanical Sciences*, 49(5):533–553.

- Kleis, I. and Kulu, P. (2007). *Solid particle erosion: occurrence, prediction and control*. Springer Science & Business Media.
- Klever, F. et al. (2010). A design strength equation for collapse of expanded octg. *SPE Drilling & Completion*, 25(03):391–408.
- Kyriakides, S. and Corona, E. (2007). *Mechanics of offshore pipelines: volume 1 buckling and collapse*, volume 1. Elsevier.
- Laitone, J. (1979a). Aerodynamic effects in the erosion process. *Wear*, 56(1):239–246.
- Laitone, J. (1979b). Erosion prediction near a stagnation point resulting from aerodynamically entrained solid particles. *Journal of Aircraft*, 16(12):809–814.
- Levy, A. and Hickey, G. (1981). Surface degradation of metals in simulated synthetic-fuels-plant environments. Technical report, Lawrence Berkeley Lab., CA (USA).
- Levy, A. V. (1979). The role of plasticity in erosion. In *International Conference on Erosion by Liquid and Solid Impact, 5 th, Cambridge, England*, pages 39–1.
- Levy, A. V. and Chik, P. (1983). The effects of erodent composition and shape on the erosion of steel. *Wear*, 89(2):151–162.
- Meng, H. and Ludema, K. (1995). Wear models and predictive equations: their form and content. *Wear*, 181:443–457.
- Oka, Y. and Yoshida, T. (2005). Practical estimation of erosion damage caused by solid particle impact: Part 2: Mechanical properties of materials directly associated with erosion damage. *Wear*, 259(1):102–109.
- Parsi, M., Najmi, K., Najafifard, F., Hassani, S., McLaury, B. S., and Shirazi, S. A. (2014). A comprehensive review of solid particle erosion modeling for oil and gas wells and pipelines applications. *Journal of Natural Gas Science and Engineering*, 21:850–873.
- Pereira, G. C., de Souza, F. J., and de Moro Martins, D. A. (2014). Numerical prediction of the erosion due to particles in elbows. *Powder Technology*, 261:105–117.
- Petrowiki.org. Perforating design. last checked: 18-11-2017. http://www.petrowiki.org/Perforating_design.
- Sharcnet.ca. Solid187 - 3-d 10-node tetrahedral structural solid. last checked: 19-11-2017. https://www.sharcnet.ca/Software/Ansys/17.0/en-us/helpans_thry/thy_el187.html.
- Smeltzer, C., Gulden, M. E., and Compton, W. (1970). Mechanisms of metal removal by impacting dust particles. *Journal of basic engineering*, 92(3):639–652.
- Sovonex.com. Api casing grades - an overview. last checked: 18-11-2017. <http://www.sovonex.com/drilling-equipment/api-casing/api-5ct-casing-grades/#common-application-casing-h40-j55-k55-m65-n80-r95>.

Stachowiak, G. and Batchelor, A. W. (2013). *Engineering tribology*. Butterworth-Heinemann.

Tilly, G. (1973). A two stage mechanism of ductile erosion. *Wear*, 23(1):87–96.